Journal of Molecular Liquids 240 (2017) 708–716

Contents lists available at ScienceDirect

Journal of Molecular Liquids

journal homepage: www.elsevier.com/locate/molliq

A combined molecular dynamics simulation, atoms in molecule analysis and IR study on the biologically important bulk fluorinated ethanols to understand the role of weak interactions in their cluster formation and hydrogen bond network

Saptarsi Mondal, Biswajit Biswas, Sunipa Sarkar, Prashant Chandra Singh *

Department of Spectroscopy, Indian Association for the Cultivation of Science, Kolkata 700032, India

ARTICLE INFO

Article history:
Received 10 March 2017
Received in revised form 15 May 2017
Accepted 22 May 2017
Available online 23 May 2017

ABSTRACT

The unique physicochemical nature of the fluorocarbon group makes fluorinated alcohols an interesting class of molecules which have diverse applications from the field of biology to chemical industries. In this paper, we have performed molecular dynamics (MD) simulation, atoms in molecule analysis (AIM) as well as IR study on the two biologically important fluorinated alcohols, trifluoroethanol (TFE) and hexafluoroisopropanol (HFIP) as well as compared them with ethanol (ETH) in order to understand the cluster formation as well as hydrogen bond network in their respective bulk media. The cluster size calculation shows that HFIP prefer to form smaller clusters than TFE and ETH. We have found the evidence of weak fluorous (F···F) interaction in TFE and HFIP by the radial distribution function (rdf) calculations and the extent of interaction is more significant in the case of HFIP which has also been confirmed by the AIM analysis. Significant amount of weak CH···F as well as C—H···O interactions have been found to contribute in the cluster formation of the bulk HFIP, whereas, only CH···F interaction was evident in the case of bulk TFE. The rdf data shows that O—H···O and O—H···F hydrogen bonds are the main contributors in the hydrogen bond network of TFE and HFIP. However, the number as well as the strength of O—H···O hydrogen bond is significantly less for HFIP compared to TFE and the strength of O—H···F hydrogen bond is more for HFIP. Due to the presence of less as well as weak O—H···O hydrogen bond in HFIP, its average hydrogen bond strength is less as compared to TFE and ETH which is also reflected by the experimental IR data of HFIP which is significantly blue shifted as compared to TFE. The MD simulation, AIM analysis and IR data clearly indicate that the organic fluorine plays significant role in the cluster formation and hydrogen bond network of TFE and HFIP through the formation of weak O—H···F hydrogen bond along with the fluorous interaction.

1. Introduction

The presence of fluorocarbon group in fluorinated alcohols endues them unusual but important chemical properties as compared to non-fluorinated alcohols [1–5]. The electronegativity of fluorine is higher as compared to hydrogen which makes the C—F group less polarizable as compared to the C—H group. Moreover, the dipole moment of C—F group is high and the direction is opposite to the C—H group [6,7]. Due to the high electronegativity and different dipole moment of the C—F group, the fluorinated molecules are extremely hydrophobic, inert as well as exhibit phase segregation properties. Indeed, fluorinated alcohols are known as environmentally compassionate solvents due to their low boiling as well as high melting point as compared to non-fluorinated analogues and hence, they have been extensively used for the plastic as well as polymer industries [8].

Trifluoroethanol (TFE) and hexafluoroisopropanol (HFIP) are two important fluorinated alcohols which have been extensively used in the polymer industry, separation techniques, pharmaceuticals, organic synthesis as well as biology [9–14]. Several unique organic reactions have been reported which are selective as well as their yields are more when they are performed in TFE and HFIP [6,7]. It has been found that the secondary structure of proteins is more stable in fluorinated alcohols-water mixture as compared to the bulk water and non-fluorinated alcohols-water mixtures [11,14]. Based on several experimental and simulation studies, it has been suggested that fluorinated alcohols show the preferential aggregation with them through fluorous interaction (F···F) around the protein by displacing water near the protein binding site which increases the probability of inter-protein hydrogen bonds [13,15]. Indeed, in another example, it has been found that probe molecules containing the C—F group get stabilized in TFE by

* Corresponding author.
E-mail address: sppcs@iacs.res.in (P.C. Singh).

http://dx.doi.org/10.1016/j.molliq.2017.05.098
0167-7322/

virtue of the fluorous interaction between the fluorine of probe and TFE [16]. These studies clearly show that fluorous interaction plays a crucial role in the stability of molecules in fluorinated alcohols.

Several experimental and theoretical efforts have been devoted to understand the different physical as well as thermodynamic properties of the aqueous mixtures of fluorinated alcohols, mainly to the TFE [17–24]. The composition-dependent compressibility, partial molar volume, density, and excess free energy of aqueous mixture of TFE indicate maximum TFE aggregation at 0.15 mol fraction of TFE [21]. X-ray and NMR studies have shown that the aggregation of TFE is more than methanol and ETH in their aqueous mixtures [25]. Several molecular dynamics (MD) simulations have been performed to understand the microheterogeneity as well as physical properties of the aqueous mixtures of TFE. Chitra et al. performed the simulation study on the aqueous mixture of TFE and reproduced all the experimental thermodynamic parameters and attributed the aggregation properties of TFE for the deviation from the ideal behavior [26]. Jalili et al. have shown that the addition of TFE increases the water structure; however, the hydrogen bond between TFE and water is broken when TFE is diluted with water [17]. HFIP-water mixture has been explored less than the TFE-water mixture. The structural fluctuations as well as aggregation of the aqueous HFIP mixtures have been studied by the NMR, X-ray and mass spectroscopic techniques [18,27]. These all studies agreed that fluorinated alcohols prefer to aggregate in their aqueous mixtures. However, the nature of different type of interactions as well as role of organic fluorine which causes the structural heterogeneity as well as hydrogen bond network of the pure TFE and HFIP in their respective bulk media have not been explored much.

In this paper, we have studied the structure as well as hydrogen bond network of the bulk TFE and HFIP as well as compared them with ETH using the MD simulation, density functional theory (DFT), atoms in molecule (AIM) analysis and IR study. The radial distribution function, g(r) have been calculated among different interacting groups to understand the reason behind the different type of cluster formation. Further, we have characterized the different cluster structures obtained from the MD simulation using the DFT with polarized continuum model (PCM). The nature of interactions has been characterized by the AIM study. It has been found that HFIP prefer to form smaller size of clusters as compared to TFE and ETH. The results show that apart from the O—H···O and O—H···F hydrogen bonds, fluorous interaction plays a pivotal role in the structure as well as microheterogeneity of TFE. Indeed, we have found that the contribution of fluorous interaction is more significant in the case of bulk HFIP than TFE. Apart from that, we have also found the evidence of several weak C—H···O as well as C—H···F interactions which contribute to the cluster formation as well as hydrogen bond network of the bulk TFE and HFIP.

2. Methods

MD simulations of ETH, TFE and HFIP have been carried out using the all atom simulation method incorporated in GROMACS molecular dynamics simulation package [28]. For ETH, all atom Amber99sb-ildn force field parameters available in the GROMACS topology were used. For TFE, we have used the Amber99sb-ildn force field parameters proposed by the Fironi et al. and modified by Gerig et al. to include the non-bonding effects of fluorine [12,20]. We have created the Amber99sb-ildn force field parameters for HFIP using its GROMOS96 force field parameters of HFIP proposed by Fironi et al. The reliability of the force field for HFIP was assured by attaining the correct density of HFIP via tuning of its partial charges [29]. Each simulation box has ~2500 alcohol molecules. For each case, we have run 1000 steps of steepest descent followed by 10,000 steps of conjugate gradient energy minimization algorithm to exclude all unfavorable interactions from the initial configuration. Each trajectory was further equilibrated in an NVT ensemble at 800 K for 200 ps to remove the biased dependencies on the initial configuration followed by an equilibration in NPT ensemble at 300 K temperature and 1 bar pressure for 500 ps. Subsequently, the equilibrated configuration was subjected to a production run of another 5 ns in NPT ensemble at 300 K and 1 bar pressure. The temperature and pressure were kept constant using the Berendsen thermostat [30] with a time constant (τ) of 0.1 ps^{-1} and the Parinello–Rahman barostat [31] with a τ of 1.0 ps^{-1}, respectively. Each simulation used a time step of 2 fs with periodic boundary condition. Neighbor list generation has been performed with the help of non-bonded force calculation with a grid and updated after every 5 steps. A cut-off radius of 1.2 nm was used both for neighbor list and van der Waal's interaction. The cluster analysis has been performed using the g_clustsize tool incorporated in the GROMACS. Two alcohol molecules are considered as a cluster if the distance between the oxygen atoms are less than the first minima of the oxygen-oxygen radial distribution function of alcohols. The coordination number (CN) for different interactions has been calculated using the default program available in the GROMACS.

The different types of clusters of ETH, TFE and HFIP up to tetramer size have been optimized in their bulk media using the B3LYP method with 6-311++G(d, p) basis set. The solvent effect in the optimization has been incorporated using the polarizable continuum model (PCM). Frequency calculations have been performed for all the structures in their bulk media in order to confirm the nature of optimized structures. The frequencies were found to be real for all the structures assuring that the particular structure is a minimum energy structure. In order to get the reliable scaling factor for the OH stretch of alcohols, we have also performed the anharmonic frequency calculation for the monomer and dimer of the alcohols. The scaling factor of 0.96 has been used for IR spectrum of the OH stretch of ETH, TFE and HFIP. Optimization has been performed with standard convergence criteria and frozen core approximation. We have also calculated the weighted average IR spectra for each size of clusters in which the weight for each cluster has been estimated from the Gibbs free energies of the respective cluster. All the calculations have been performed using the G09 suites of program [32]. Further, AIM calculations have been performed to characterize the nature of interaction between different groups of alcohols [33].

Fourier transform infrared spectrometer (Nicolet iS10, Thermo Fisher) operating in the attenuated total reflection mode (ATR) has been used to measure the IR spectra of alcohols. The resolution of IR measurement was 2 cm^{-1}. The ATR correction has been performed for all IR spectra. N_2 gas was flown throughout the measurement to remove the effect of atmospheric vapors. All the measurements have been performed at room temperature (25 ± 3 °C).

3. Results and discussion

3.1. Molecular dynamics simulation

Fig. 1 shows the snapshot of bulk ETH, TFE and HFIP within the 6 Å. Generally, the snapshot of only one microstate of a system does not provide serious information. However, in this case, it can be visualized that the OH group of fluorinated–ETHs (TFE and HFIP) comes closer to OH as well as C—F group of other molecules, whereas, oxygen end of ETH comes closer to each other through the formation of O—H···O hydrogen bond. Apart from that, the C—F group of TFE and HFIP comes closer to the other C—F group of molecules. It is also apparent from the snapshots that the number of fluorocarbon groups approaching towards the fluorine terminal is higher for HFIP than TFE. The snapshots of fluorinated-ETHs clearly indicate that apart from the OH group, fluorocarbon group of fluorinated-ETHs also plays a significant role in their heterogeneous environments.

Fig. 2 shows the radial distribution function g(r) for the different sites (OH, CH_3/CF_3 and CH_2/CH terminals) of ETH, TFE and HFIP. The g(r) between the oxygen and hydrogen of the OH of ETH (Fig. 2a, red line) shows a first peak at 1.88 Å depicting the intermolecular O—H···O hydrogen bond in the bulk ETH. This result is in well accordance with earlier MD simulations [34,35]. The g(r) between the

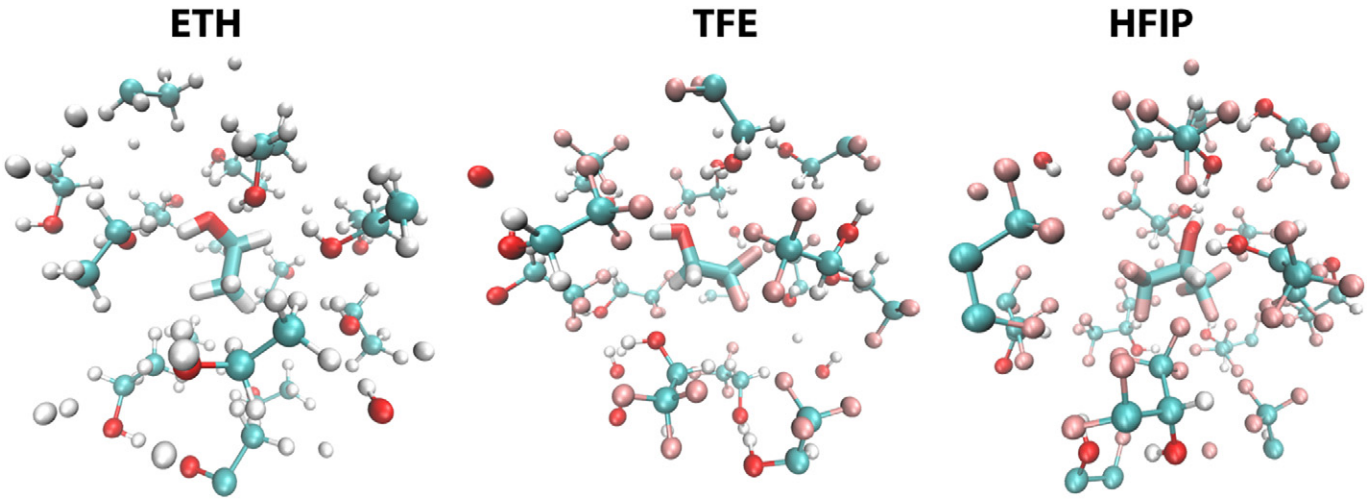

Fig. 1. Snapshots of the bulk ETH, TFE and HFIP within 6 Å obtained from the MD simulation run.

oxygen and hydrogen of the OH of TFE (Fig. 2a, dark yellow line) shows first peak at 1.87 Å indicating that the intermolecular O—H···O hydrogen bond is marginally stronger in the bulk TFE. Interestingly, the g(r) between the oxygen and hydrogen of the OH for HFIP (Fig. 2a, sky blue line) shows first peak at 1.97 Å, which is longer compared to the case of ETH (1.88 Å) and TFE (1.87 Å) indicating that the strength of O—H···O hydrogen bond in bulk HFIP is significantly weaker than TFE and ETH. Intensity of the first peak of the g(r) between the oxygen and hydrogen of the OH for HFIP is almost half as compared to ETH and TFE indicating that the number of O—H···O hydrogen bond is significantly less in HFIP than ETH and TFE. We have also investigated the probability of interaction between the OH and fluorine of fluorinated

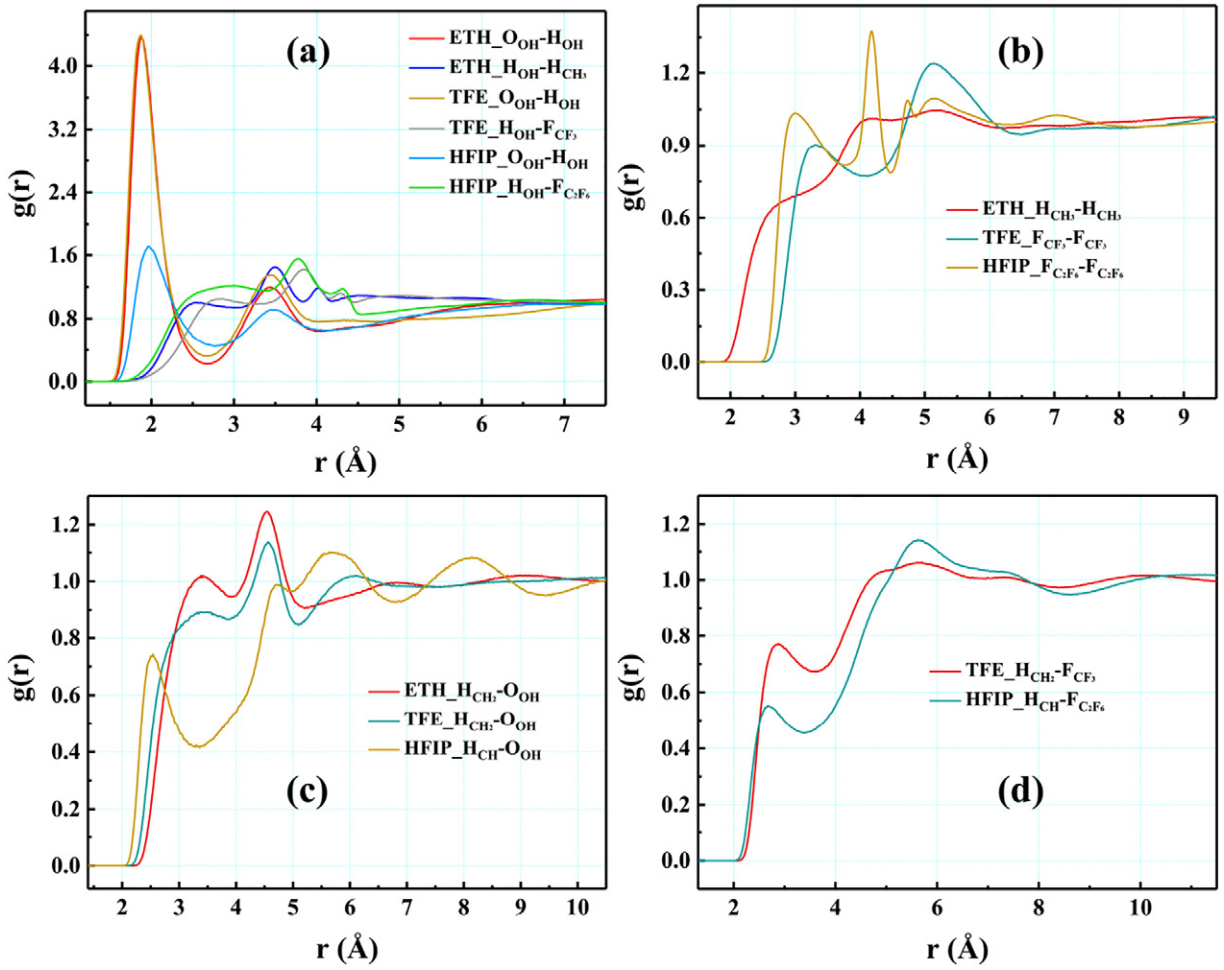

Fig. 2. (a) g(r) between oxygen and hydrogen of the OH group of ETH, TFE and HFIP as well as g(r) between hydrogen of OH and hydrogen of ETH along with fluorine of TFE and HFIP. (b) g(r) between the CH_3 of ETH and CF_3 of TFE and HFIP. (c) g(r) between the hydrogen of CH_2/CH and oxygen of the OH of ETH, TFE and HFIP. (d) g(r) between the hydrogen of CH_2/CH and fluorine of TFE and HFIP.

alcohols by calculating the g(r) between these sites of fluorinated ETHs. The g(r) for TFE (Fig. 2a, grey line) shows first peak at 2.78 Å, whereas, comparatively broad first peak at 2.62 Å was observed for HFIP (Fig. 2a, green line). We have also calculated the g(r) between the hydrogen of –CH_3 and OH of ETH (blue line, Fig. 2a) and it shows sharp first peak around the 2.6 Å, however, its intensity is less compared to the g(r) of TFE and HFIP for O—H···F contacts which shows that less number of –CH_3 comes closer to the OH group of ETH than fluorine in the case of TFE and HFIP. In bulk ETH, hydrogen of –CH_3 and OH is coming closer, however, it is less probable that they are interacting with each other because of similar nature of charge on the hydrogen. The g(r) calculations reveal that apart from the O—H···O hydrogen bond, significant amount of O—H···F interaction exists for the bulk TFE and HFIP. It has been found that the number as well as strength of the O—H···O hydrogen bond in HFIP is significantly less compared to TFE, whereas, the contribution of the O—H···F interaction is comparatively higher for HFIP than TFE which indicates that the role of fluorine is more significant in the cluster formation of bulk HFIP than TFE.

The g(r) calculation for the –CH_3 terminal of ETH does not show any peak which indicates that the probability of specific CH_3···CH_3 interaction is very less. In contrast to ETH, first peak of g(r) of the CF_3 terminal of TFE (3.2 Å) and HFIP (3.0 Å) shows a sharp feature within 3.5 Å indicating the presence of the fluorous (F···F) interaction in the bulk TFE and HFIP (Fig. 2b). The intensity of the first peak of g(r) between CF_3 terminals for HFIP is higher and the distance is shorter compared to TFE indicating that the strength as well as number of fluorous interaction is higher for HFIP than TFE. The g(r) calculations between the CH_2 and oxygen of ETH and TFE shows first peak beyond 3.5 Å indicating that the CH_2···O interaction is insignificant in their bulk media. However, a sharp first peak appears around 2.4 Å for the g(r) between the CH and oxygen of HFIP indicating the possibility of weak CH···O interaction in the bulk HFIP (Fig. 2c). Similarly, g(r) calculations between the CH_2/CH and fluorine for TFE and HFIP shows first peak at 2.9 and 2.7 Å respectively, suggesting the presence of CH_2/CH···F interaction in the bulk TFE and HFIP (Fig. 2d). MD simulations clearly reveal the presence of several weak interactions (O—H···F, F···F, CH···F) apart from the strong O—H···O hydrogen bond which contributes to the cluster formation of the bulk TFE and HFIP.

Fig. 3 shows the probability of the cluster size distribution for ETH, TFE and HFIP at their oxygen sites. It can be clearly seen that the cluster size distribution decays exponentially from n = 1 for all alcohols. For the simple liquid, it is intuitively apparent that single species probability is significant and the probability will decrease rapidly with the increase of cluster size [36]. Interestingly, the probability of single cluster for the HFIP is higher as compared to the ETH and TFE. However, the probability of bigger cluster for HFIP decreases sharply as compared to ETH and TFE.

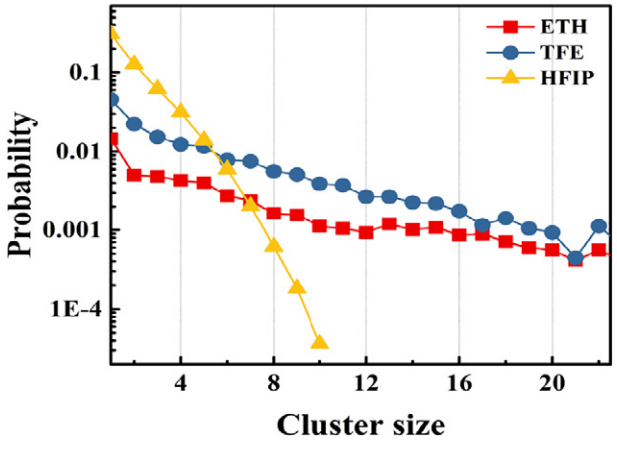

Fig. 3. Oxygen site cluster probability of ETH, TFE and HFIP calculated using the g_cluster size option present in the MD simulation.

The tendency of HFIP to form small clusters is probably due to the steric factor as the OH of HFIP is between two bulky CF_3 groups whereas the OH group of ETH and TFE are present at the terminal. We have found that these observations are robust irrespective of the choice of cut off distances used for the cluster size calculation.

Further, we have calculated CN for the different mode of interactions of alcohols and their values are shown in Table 1. It can be seen that the CN for the O—H···O hydrogen bond is maximum for ETH and it decreases with the increase of fluorination. The CN for the O—H···F interaction is higher for the HFIP as compared to the TFE. Similarly, the CN for the F···F interaction is more for HFIP than TFE. For CH···O/F interactions, the value of CN for HFIP is less than TFE which is because of the steric hindrance as the CH group of HFIP is between two CF_3 groups. The trend in the CN for the different interactions are in the well agreement with the results obtained from g(r) calculations.

3.2. Density functional theory and AIM calculations

The g(r) and cluster data obtained from the MD simulations clearly establish the interaction responsible for the heterogeneity of ETH, TFE and HFIP. However, g(r) calculations only tell about the possibility of different interactions and it does not provide any insight information about the nature of interactions. Hence, to understand the nature of interactions, it is desirable to obtain the information about the structure as well as different interactions at the cluster level. Fig. 4 shows the optimized structures of alcohols up to four molecules along with the important intermolecular distances obtained at the B3LYP/6-311++G(d, p) level of theory coupled with the PCM model. The relative energy and population of the different clusters of alcohols are shown in Table S1. ETH monomer exists in gauche and trans forms in the bulk medium with almost equal energy. The ETH dimers form linear intermolecular O—H···O hydrogen bonded structure. The most stable structure of trimer of ETH is linear O—H···O hydrogen bonded complex, whereas, the most stable and populated structure for the tetramer and pentamer clusters of ETH have cyclic O—H···O hydrogen bond in their bulk medium. Indeed, in earlier theoretical studies, it has been predicted that the small size of ETH clusters are linear and big size of clusters form ring in the bulk medium [37].

TFE monomer exists in gauche and trans form and the relative energy of the gauche form is slightly higher (0.5 kcal/mol) compared to the trans conformer in its bulk media. The relative population of the gauche form (67%) is higher compared to the trans (33%). Earlier, diffraction studies on the bulk TFE have established the presence of ~40% trans conformer which is in close agreement with the present calculation [38]. The most stable dimer structure of TFE is linear O—H···O hydrogen bonded complex, similar to ETH, however, the O—H···O distance is less than ETH. The other structures of the TFE dimer have the intermolecular O—H···F contact, however, the populations of these structures are less than the O—H···O hydrogen bonded clusters. Indeed, it has been reported by the jet cooled study of the TFE clusters that the O—H···O hydrogen bond is the main driving force for the dimer formation of TFE along with secondary O—H···F contacts [39]. The trimer and tetramer clusters of the TFE are cyclic structures having the O—H···O hydrogen bond and O—H···F contacts. The HFIP exists in antiperiplanar (AP) and synclinal (S) conformation in their bulk medium in which the stability and

Table 1
Coordination number (CN) for the different interaction of ETH, MFE and TFE calculated by the MD simulation.

Interaction ETH	CN	Interaction TFE	CN	Interaction HFIP	CN
O_{OH}···H_{OH}	0.94	O_{OH}···H_{OH}	0.80	O_{OH}···H_{OH}	0.36
H_{OH}···H_{CH_3}	2.33	H_{OH}···F_{CF_3}	2.39	H_{OH}···$F_{C_2F_6}$	4.88
O_{OH}···H_{CH_2}	3.45	O_{OH}···H_{CH_2}	2.49	O_{OH}···H_{CH}	0.34
H_{CH_3}···H_{CH_3}	2.42	F_{CF_3}···F_{CF_3}	3.83	$F_{C_2F_6}$···$F_{C_2F_6}$	4.60
		H_{CH_2}···F_{CF_3}	2.38	H_{CH}···$F_{C_2F_6}$	1.90

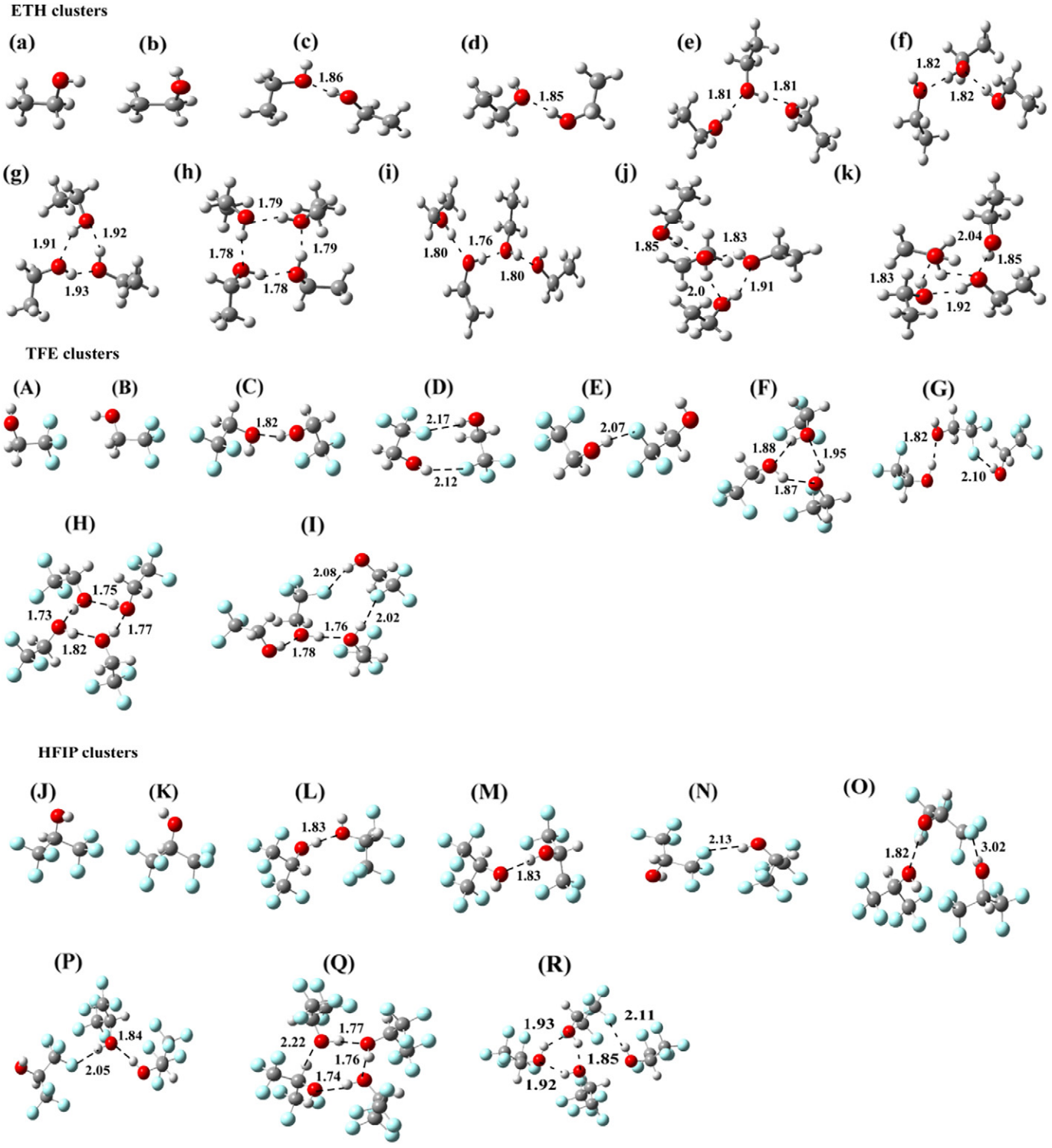

Fig. 4. The optimized structures of ETH, TFE and HFIP clusters in their respective bulk media using the B3LYP/6-311++G(d, p) level of theory. The solvent effect has been added using the PCM method. The carbon, hydrogen, oxygen and fluorine atoms are depicted in ash, white, red and light blue colors, respectively. The unit of intermolecular (black line) distances is in Å.

population of AP form is higher than S. Earlier bulk as well as matrix isolation studies also predicted that the AP form of the HFIP is more stable as compared to the S form [40,41]. Similar to TFE clusters, HFIP clusters are stabilized by the O—H···O hydrogen bonds as well as O—H···F interactions. For TFE and HFIP, apart from the O—H···O hydrogen bond and O—H···F interaction, there are significant amount of C—H···F and F···F interactions present within the distance of 3 Å (Fig. S1) which is in accordance with the results obtained from the MD simulation of fluorinated-ETHs.

Further, AIM analysis on the different size of clusters of alcohols in their bulk media has been performed in order to ensure the nature of several interactions observed in their optimized structures. Figs. 5 and S2 show the molecular graph of the electron density for the structures of different size of clusters of alcohols. The values of the electron density

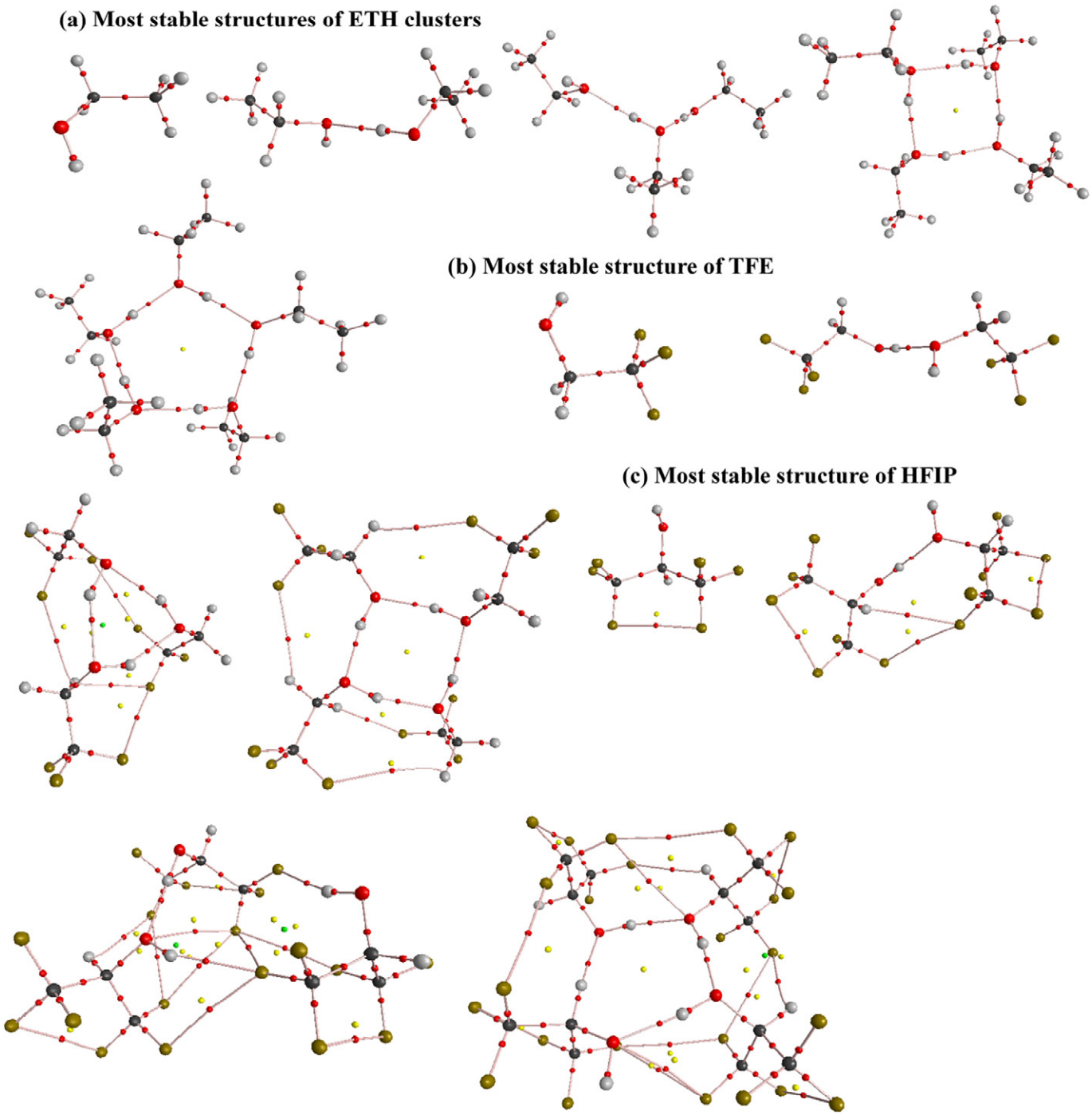

Fig. 5. Molecular graph of the topology of the electron density for the most stable structures of ETH, TFE and HFIP clusters in their respective bulk media calculated at the B3LYP/6-311++G(d, p) level of theory.

(ρ), Laplacian (∇^2), total electronic energy density (H) as well as its components, local electronic kinetic energy (G) and potential energy (V) densities at bond critical points (BCP) are shown in Table S2. A (3, −1) BCP with a positive Laplacian indicates the presence of noncovalent interaction, whereas, the presence of a (3, +1) ring critical point (RCP) along with a BCP shows that the corresponding structure is cyclic in nature. The values of topological parameters shown in Table S2 are in the range of acceptable values for the non-covalent interaction [42–46]. The linear structures of ETH have the (3, −1) BCP, whereas, the close structures show the (3, +1) RCP along with the (3, −1) BCP ensuring their cyclic nature. Earlier, the g(r) calculations between hydrogen of CH_3 and OH indicates that they come closer to each other, however, we could not find any BCP between these two atoms indicating that there is no interaction exist between them.

We could not find any BCP for the intramolecular O—H···F hydrogen bonds indicating that intramolecular O—H···F hydrogen bond is absent in bulk TFE. The linear hydrogen bonded clusters of TFE shows (3, −1) BCP for the O—H···O and O—H···F contacts indicating that these contacts are hydrogen bonded. The values of topological parameters for the O—H···O interaction are higher than O—H···F contacts indicating that the strength of the O—H···F interaction is less compared to the O—H···O interaction. Most interesting observation is the presence of the (3, −1) BCP for the intermolecular F···F as well as CH_2···F interactions and the topological parameters are well in the range of non-

covalent interaction. For example, the structure G (Fig. S2) of TFE dimer shows two F···F interactions along with the O—H···F interaction and because of the F···F interactions, AIM analysis shows two (3, +1) ring BCP which make this structure cyclic. For the higher order clusters, number of CH···F interaction as well as F···F interactions increases which is evident from the presence of (3, +3) cage critical points in the tetramer clusters of TFE which is in accordance with the MD simulation results discussed earlier.

The AP and S conformers of HFIP shows a BCP for the F···F interaction and the values of topological parameters for this interaction in AP is slightly higher than S indicating that the weak F···F interaction plays an important role in the higher stability of AP form of HFIP in its bulk medium. Similar to the TFE, there is no BCP between the O—H and the fluorine within a HFIP molecule indicating that intramolecular O—H···F interaction is absent in the bulk HFIP. The higher order of HFIP clusters show BCPs for the O—H···O and O—H···F hydrogen bond along with the F···F as well as CH···F interactions. The number of F···F interaction in any particular size of clusters for HFIP is higher compared to TFE due to which HFIP shows more number of (3, +1) ring BCP than TFE. It is also noticeable that the values of topological parameters for the F···F interaction are higher for HFIP than TFE which demonstrates that the fluorous interaction is more significant in the stabilization of the HFIP which is in accordance with the results of MD simulations discussed above. In summary, bulk ETH clusters are stabilized by the O—H···O hydrogen bond, whereas, O—H···O and O—H···F hydrogen bonds along with the weak fluorous interaction which are dispersive in the nature stabilize the bulk TFE and HFIP clusters and the extent of fluorous interaction is more significant for the bulk HFIP.

3.3. IR studies

The OH stretching frequency of alcohols is extremely sensitive to the local environment; hence, it can be employed to understand the hydrogen bond network of alcohols. Fig. 6 shows the IR spectra of ETH, TFE and HFIP in their OH stretching region. The peak position of the OH stretch of the ETH, TFE and HFIP appears at the 3308, 3335, 3418 cm^{-1}, respectively. The IR spectra of fluorinated-ETHs get successively blue shifted compared to ETH indicating that the average hydrogen bond strength of fluorinated-ETHs is less than ETH. The amount of blue shift for HFIP (110 cm^{-1}) is significantly high compared to TFE (27 cm^{-1}) indicating that the weakening of hydrogen bond is more incisive in HFIP than TFE. Apart from the blue shift, TFE shows additional peak at the 3632 cm^{-1} whereas HFIP shows two additional peaks at 3592, 3632 cm^{-1}. It is important to mention here that earlier IR studies of the bulk TFE and HFIP show an additional peak at 3680 cm^{-1} which is absent in our case [21,47,48]. The peak appearing at 3680 cm^{-1} in the earlier IR studies is due to the contamination of water in fluorinated-ETHs. The appearance of peaks in the high frequency region of the OH stretch of fluorinated ETHs suggest the presence of extremely weak hydrogen bonded species in TFE and HFIP, which is absent in the case of ETH. MD simulations as well as AIM calculations clearly show that the TFE and HFIP can form weak O—H···F hydrogen bond along with strong O—H···O hydrogen bond. Hence, the peak observed in the high frequency region of the OH stretch of TFE and HFIP can be tentatively assigned to the weak O—H···F hydrogen bonded species.

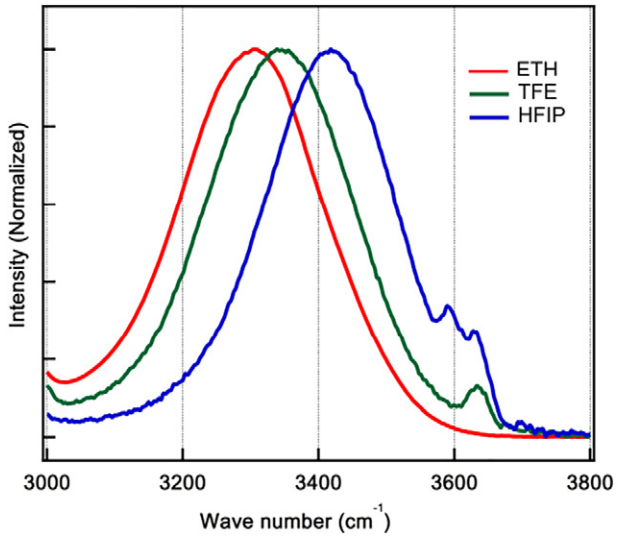

Fig. 6. IR spectra of the OH stretch of ETH (red), TFE (green) and HFIP (blue).

In order to ensure the assignments of the observed IR peaks, we have performed the IR calculation for each size of clusters of ETH, TFE and HFIP in their bulk media (Table S3) as well as calculated their weighted average IR spectra as shown in the Fig. 7. The weighted average IR spectrum of the monomer of ETH shows a peak at 3630 cm^{-1}, however, the experimental IR spectrum of the OH stretch of ETH does not show any feature in that region which suggest that ETH does not exist in the monomer form in their bulk media. It can be seen that the vibrational band positions of the O—H···O hydrogen bonded clusters of alcohols get more red shifted with the increase of the cluster size as compared to their free OH stretching frequency. Indeed, earlier supersonic jet study on the different size of clusters for the ETH and TFE shows that the OH frequency gets shifted to lower frequency with the increase of the cluster size due to increased cooperativity of the O—H···O hydrogen bond [49]. It is noticeable that the monomer of TFE and HFIP shows the OH stretch around ~3640 cm^{-1} which is close to the observed experimental feature at ~3620 cm^{-1} of TFE and HFIP. However, the observed experimental band shape is comparatively broad unlike the sharp IR feature of isolated monomer as observed in the gas phase experiments. Moreover, we could not find any isolated monomer of TFE and HFIP in our simulations. Hence, the peak observed around 3600 cm^{-1} in the TFE and HFIP cannot be assigned to their isolated monomer. The weighted average IR spectra of dimer and trimer of TFE shows a vibrational feature at high frequency around ~3620 cm^{-1} which is close to the observed experimental feature at 3632 cm^{-1} and has been assigned to the weak O—H···F hydrogen bond. Similarly, due to the weak O—H···F hydrogen bond, the IR spectra of dimer and trimer of HFIP also show double peak feature around 3598 and 3616 cm^{-1} which is close to observed experimental features at 3592, 3632 cm^{-1}. Infact, earlier study on the dimer and trimer of the TFE in the supersonic jet condition also shows a peak ~3630 cm^{-1} which has been assigned to the O—H···F interaction between the TFE clusters [39,49]. Hence, the weak feature appearing in the 3600 cm^{-1} region for HFIP and TFE has been tentatively assigned to the weak intermolecular O—H···F hydrogen bonds mainly arising from the dimer and trimer of fluorinated-ETHs, whereas, the strong broad band appearing below 3580 cm^{-1} has been assigned to the O—H···O hydrogen bonded clusters of alcohols in their bulk media. From the MD simulation and IR measurements, it is clear that the number as well as strength of O—H···O hydrogen bond in TFE is almost same to the ETH; however, a small population of weak O—H···F hydrogen bond exists in the TFE which makes the overall strength of hydrogen bond slightly weaker as compared to the ETH. In the case of HFIP, number as well as strength of O—H···O hydrogen bonds decrease to almost half and strength of O—H···F hydrogen bond is increased as compared to the TFE which drastically decreases the average strength of hydrogen bond for HFIP hence, the IR spectrum shows a significant blue shift as compared to ETH and TFE.

4. Conclusion

We have performed MD simulation, DFT calculation coupled with AIM analysis and IR measurements to investigate the cluster formation as well as hydrogen bond network of biologically important bulk TFE

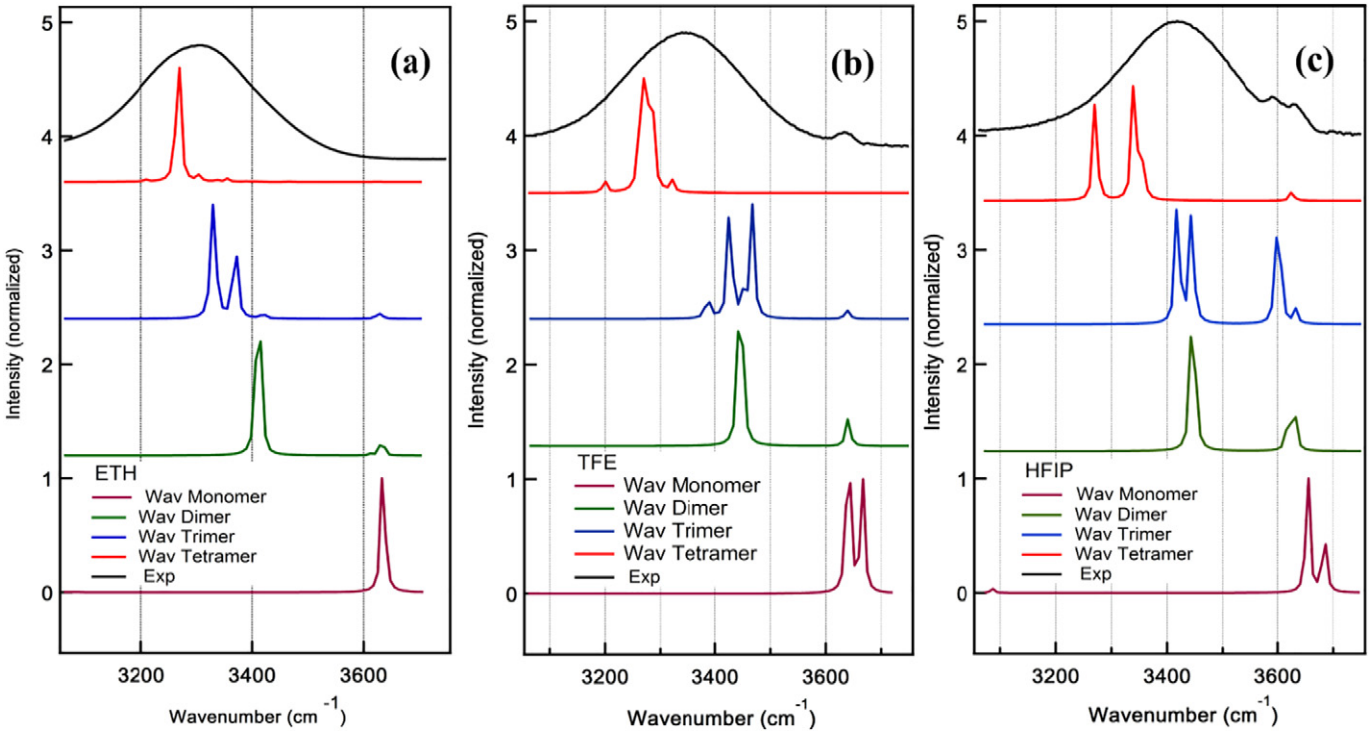

Fig. 7. The calculated IR spectra of the different size of clusters in the OH stretching region of ETH (a), TFE (b) and HFIP (c) in their respective bulk media. Black line in each panel shows the experimental IR data of the respective alcohols in the OH stretching region.

and HFIP. Further, we have compared the results with bulk ETH to understand the role of fluorocarbon in the structure as well as hydrogen bond network of the TFE and HFIP. Cluster size distribution analysis clearly shows that the HFIP prefers to form small clusters, whereas, TFE and ETH forms comparatively bigger clusters. The g(r) between the oxygen and hydrogen of the OH of all alcohols indicate that the strength as well as number of O—H···O hydrogen bond in ETH and TFE are very similar; however, the strength and number of O—H···O hydrogen bond in HFIP are significantly less as compared to ETH and TFE. The g(r) between the hydrogen of OH and the fluorine of CF_3 for TFE and HFIP shows first peak within 3 Å depicting the presence of weak O—H···F interaction in TFE and HFIP. The AIM analysis confirms the presence of O—H···F and O—H···O hydrogen bonds in TFE and HFIP. Presence of the less number of O—H···O as well as O—H···F hydrogen bonds decreases the average hydrogen bond strength of HFIP compared to TFE and ETH which is also verified by the experimental IR data of the OH stretch of HFIP which shows a significant blue shift compared to ETH and TFE. Further, g(r) and AIM analysis confirm the presence of fluorous interaction in the bulk HFIP as well as TFE. It has been found that the role of fluorous interaction is more prominent in the case of HFIP compared to TFE. We have also found the evidence of the presence of weak CH···O as well as CH···F interactions in the bulk HFIP, whereas, only CH···F interaction has been found for the bulk TFE. The IR results along with the MD simulation and AIM analysis establish that the organic fluorine plays a crucial role in the cluster formation of TFE, HFIP through the formation of weak O—H···F hydrogen bond along with the dispersive fluorous interaction.

Acknowledgements

This work is supported partially by the research grants provided by the Council of Scientific and Industrial Research (CSIR) [Grant No. 01(2803)/14/EMR-II] as well as Department of Science and Technology (DST-SERB) [Grant No. EMR/2015/001605] India. S. M., B. B. and S. S. thank institute, CSIR and DST respectively for the fellowships.

Appendix A. Supplementary data

The details of AIM and frequency analysis are provided in the supporting information.

Supplementary data associated with this article can be found in the online version, at http://dx.doi.org/10.1016/j.molliq.2017.05.098.

References

[1] E.N.G. Marsh, Fluorinated proteins: from design and synthesis to structure and stability, Acc. Chem. Res. 47 (2014) 2878–2886.
[2] W.-Q. Deng, V. Molinero, W.A. Goddard, Fluorinated imidazoles as proton carriers for water-free fuel cell membranes, J. Am. Chem. Soc. 126 (2004) 15644–15645.
[3] P. Zhou, J. Zou, F. Tian, Z. Shang, Fluorine bonding — how does it work in protein—ligand interactions? J. Chem. Inf. Model. 49 (2009) 2344–2355.
[4] B. Biswas, S. Mondal, P.C. Singh, Combined molecular dynamics, atoms in molecules, and IR studies of the bulk monofluoroethanol and bulk ethanol to understand the role of organic fluorine in the hydrogen bond network, J. Phys. Chem. A 121 (2017) 1250–1260.
[5] B.C. Buer, E.N.G. Marsh, Fluorine: a new element in protein design, Protein Sci. 21 (2012) 453–462.
[6] E. Clot, O. Eisenstein, N. Jasim, S.A. Macgregor, J.E. McGrady, R.N. Perutz, C—F and C—H bond activation of fluorobenzenes and fluoropyridines at transition metal centers: how fluorine tips the scales, Acc. Chem. Res. 44 (2011) 333–348.
[7] M.E. Evans, C.L. Burke, S. Yaibuathes, E. Clot, O. Eisenstein, W.D. Jones, Energetics of C—H bond activation of fluorinated aromatic hydrocarbons using a [Tp'Rh(CNneopentyl)] complex, J. Am. Chem. Soc. 131 (2009) 13464–13473.
[8] T. Narita, Synthesis of novel fluorinated polymers: facile carbon–carbon bond formation aided by fluorine substituents, Polym. J. 43 (2011) 497–515.
[9] J.T. Gerig, Structure and solvation of melittin in 1,1,1,3,3,3-hexafluoro-2-propanol/water, Biophys. J. 86 (2004) 3166–3175.
[10] S. Jalili, M. Akhavan, A molecular dynamics simulation study of conformational changes and solvation of Aβ peptide in trifluoroethanol and water, J. Chem. Theory Comput. 08 (2009) 215–231.
[11] M. Guo, Y. Mei, Equilibrium and folding simulations of NS_4B H_2 in pure water and water/2,2,2-trifluoroethanol mixed solvent: examination of solvation models, J. Mol. Model. 19 (2013) 3931–3939.
[12] J.T. Gerig, Toward a molecular dynamics force field for simulations of 40% trifluoroethanol–water, J. Phys. Chem. B 118 (2014) 1471–1480.
[13] D. Roccatano, G. Colombo, M. Fioroni, A.E. Mark, Mechanism by which 2,2,2-trifluoroethanol/water mixtures stabilize secondary-structure formation in peptides: a molecular dynamics study, Proc. Natl. Acad. Sci. 99 (2002) 12179–12184.

[14] K. Gast, D. Zirwer, M. Müller-Frohne, G. Damaschun, Trifluoroethanol-induced conformational transitions of proteins: insights gained from the differences between α-lactalbumin and ribonuclease A, Protein Sci. 8 (1999) 625–634.
[15] S. Jalili, P. Amani, Molecular dynamics simulation study of solvation effects of water and trifluoroethanol on gamma-aminobutyric acid (GABA), J. Mol. Liq. 197 (2014) 27–34.
[16] S. Mondal, R. Halder, B. Biswas, B. Jana, P.C. Singh, Solvent organization around the perfluoro group of coumarin 153 governs its photophysical properties: an experimental and simulation study of coumarin dyes in ethanol as well as fluorinated ethanol solvents, J. Chem. Phys. 144 (2016) 184504.
[17] S. Jalili, M. Akhavan, Molecular dynamics simulation study of association in trifluoroethanol/water mixtures, J. Comput. Chem. 31 (2010) 286–294.
[18] T. To, Y. Hatomoto, T. Umecky, T. Takamuku, Solvation power of HFIP for the hydrophilic and the hydrophobic moieties of l-leucine studied by MD, IR, and NMR techniques, J. Mol. Liq. 230 (2017) 261–270.
[19] R.M. Culik, R.M. Abaskharon, I.M. Pazos, F. Gai, Experimental validation of the role of trifluoroethanol as a nanocrowder, J. Phys. Chem. B 118 (2014) 11455–11461.
[20] M. Fioroni, K. Burger, A.E. Mark, D. Roccatano, A new 2,2,2-Trifluoroethanol model for molecular dynamics simulations, J. Phys. Chem. B 104 (2000) 12347–12354.
[21] P. Morgado, A.R. Garcia, L.M. Ilharco, J. Marcos, M. Anastácio, L.F.G. Martins, E.J.M. Filipe, Liquid mixtures involving hydrogenated and fluorinated alcohols: thermodynamics, spectroscopy, and simulation, J. Phys. Chem. B 120 (2016) 10091–10105.
[22] T. Takamuku, M. Tanaka, T. Sako, T. Shimomura, K. Fujii, R. Kanzaki, M. Takeuchi, Solvation of the amphiphilic diol molecule in aliphatic alcohol—water and fluorinated alcohol—water solutions, J. Phys. Chem. B 114 (2010) 4252–4260.
[23] T. Takamuku, M. Tobiishi, H. Saito, Solvation properties of aliphatic alcohol–water and fluorinated alcohol–water solutions for amide molecules studied by IR and NMR techniques, J. Solut. Chem. 40 (2011) 2046–2056.
[24] M. Heger, T. Scharge, M.A. Suhm, From hydrogen bond donor to acceptor: the effect of ethanol fluorination on the first solvating water molecule, Phys. Chem. Chem. Phys. 15 (2013) 16065.
[25] T. Takamuku, T. Kumai, K. Yoshida, T. Otomo, T. Yamaguchi, Structure and dynamics of halogenoethanol—water mixtures studied by large-angle X-ray scattering, small-angle neutron scattering, and NMR relaxation, J. Phys. Chem. A 109 (2005) 7667–7676.
[26] R. Chitra, P.E. Smith, A comparison of the properties of 2,2,2-trifluoroethanol and 2,2,2-trifluoroethanol/water mixtures using different force fields, J. Chem. Phys. 115 (2001) 5521–5530.
[27] K. Yoshida, T. Yamaguchi, T. Adachi, T. Otomo, D. Matsuo, T. Takamuku, N. Nishi, Structure and dynamics of hexafluoroisopropanol-water mixtures by x-ray diffraction, small-angle neutron scattering, NMR spectroscopy, and mass spectrometry, J. Chem. Phys. 119 (2003) 6132–6142.
[28] E.L.D. van der Spoel, B. Hess, A.R. van Buuren, E. Apol, P.J. Meulenhoff, D.P. Tieleman, A.L.T.M. Sijbers, K.A. Feenstra, R. van Drunen, H.J.C. Berendsen, Gromacs user manual, www.gromacs.org 2014.
[29] M. Fioroni, K. Burger, A.E. Mark, D. Roccatano, Model of 1,1,1,3,3,3-hexafluoropropan-2-ol for molecular dynamics simulations, J. Phys. Chem. B 105 (2001) 10967–10975.
[30] H.J.C. Berendsen, J.P.M. Postma, W.F.v. Gunsteren, A. DiNola, J.R. Haak, Molecular dynamics with coupling to an external bath, J. Chem. Phys. 81 (1984) 3684–3690.
[31] M.P.a.A. Rahman, Polymorphic transitions in single crystals: a new molecular dynamics method, J. Appl. Phys. 52 (1981) 7182–7190.
[32] G.W.T.M.J. Frisch, H.B. Schlegel, G.E. Scuseria, M.A. Robb, J.R. Cheeseman, G. Scalmani, V. Barone, B. Mennucci, G.A. Petersson, et al., Gaussian 09 Revision B.01, Gaussian, Inc., Wallingford, CT, 2010.
[33] R.F.W. Bader, Atoms in Molecules- A Quantum Theory, Oxford University Press, USA, 1990.
[34] L. Saiz, J.A. Padró, E. Guàrdia, Structure and dynamics of liquid ethanol, J. Phys. Chem. B 101 (1997) 78–86.
[35] A. Vrhovšek, O. Gereben, A. Jamnik, L. Pusztai, Hydrogen bonding and molecular aggregates in liquid methanol, ethanol, and 1-propanol, J. Phys. Chem. B 115 (2011) 13473–13488.
[36] M. Pozar, B. Lovrincevic, L. Zoranic, T. Primorac, F. Sokolic, A. Perera, Micro-heterogeneity versus clustering in binary mixtures of ethanol with water or alkanes, Phys. Chem. Chem. Phys. 18 (2016) 23971–23979.
[37] O. Gereben, Ring structure analysis of ethanol–water mixtures, J. Mol. Liq. 211 (2015) 812–820.
[38] I. Bakó, T. Radnai, M.C.B. Funel, Investigation of structure of liquid 2,2,2 trifluoroethanol: neutron diffraction, molecular dynamics, and ab initio quantum chemical study, J. Chem. Phys. 121 (2004) 12472–12480.
[39] T. Scharge, C. Cezard, P. Zielke, A. Schutz, C. Emmeluth, M.A. Suhm, A peptide co-solvent under scrutiny: self-aggregation of 2,2,2-trifluoroethanol, Phys. Chem. Chem. Phys. 9 (2007) 4472–4490.
[40] H. Schaal, T. Häber, M.A. Suhm, Hydrogen bonding in 2-propanol. The effect of fluorination, J. Phys. Chem. A 104 (2000) 265–274.
[41] A. Shahi, E. Arunan, Microwave spectroscopic and theoretical investigations of the strongly hydrogen bonded hexafluoroisopropanol···water complex, Phys. Chem. Chem. Phys. 17 (2015) 24774–24782.
[42] B. Biswas, S. Mondal, P.C. Singh, Role of hydrogen bond in the solvation behavior of the binary mixtures containing fluorocarbon alcohol molecules and chloroform: an experimental and theoretical study, ChemistrySelect 1 (2016) 5607–5617.
[43] S. Mondal, A.U. Teja, P.C. Singh, Effect of microhydration on the atmospherically important metastable carbonyl sulfide anion: structure, energetic, and infrared study, Int. J. Quantum Chem. 115 (2015) 785–795.
[44] S. Mondal, A.U. Teja, P.C. Singh, Theoretical study on the microhydration of atmospherically important carbonyl sulfide in its neutral and anionic forms: bridging the gap between the bulk and finite size microhydrated cluster, J. Phys. Chem. A 119 (2015) 3644–3652.
[45] B. Biswas, P.C. Singh, Effect of hydration on the organo-noble gas molecule HKrCCH: role of krypton in the stabilization of hydrated HKrCCH complexes, Phys. Chem. Chem. Phys. 17 (2015) 30632–30641.
[46] S. Mondal, P. Chandra Singh, Noble gas induced surprisingly higher stability of π hydrogen bonded complex: comparative study of hydrogen bonded complexes of HKrCCH and HCCH with H_2O, NH_3, CH_3OH and CH_3NH_2, RSC Adv. 4 (2014) 20752.
[47] K.R. Harris, P.J. Newitt, Z.J. Derlacki, Alcohol tracer diffusion, density, NMR and FTIR studies of aqueous ethanol and 2,2,2-trifluoroethanol solutions at 25°C, J. Chem. Soc. Faraday Trans. 94 (1998) 1963–1970.
[48] V.F. Kalasinsky, H.V. Anjaria, Vibrational spectra and conformations of 2,2,2-trifluoroethylamine and 2,2,2-trifluoroethanol, J. Phys. Chem. 84 (1980) 1940–1944.
[49] T. Scharge, N. Wassermann Tobias, A. Suhm Martin, Weak hydrogen bonds make a difference: dimers of jet-cooled halogenated ethanols, Z. Phys. Chem. 222 (2008) 1407–1452.